Nano Energy (2015) 18, 28–36

Available online at www.sciencedirect.com

ScienceDirect

journal homepage: www.elsevier.com/locate/nanoenergy

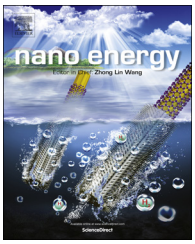

RAPID COMMUNICATION

Hybrid nanogenerators based on triboelectrification of a dielectric composite made of lead-free $ZnSnO_3$ nanocubes

Guo Wang, Yi Xi*, Haixia Xuan, Ruchuan Liu*, Xi Chen, Lu Cheng

Department of Applied Physics, Chongqing University, Chongqing 400044, PR China

Received 7 July 2015; received in revised form 2 September 2015; accepted 17 September 2015
Available online 4 October 2015

KEYWORDS
Lead-free $ZnSnO_3$ nanocubes;
PDMS;
Composite;
Triboelectric nanogenerator (TENG)

Abstract
Based on mixed piezoelectric and ferroelectric nanostructures with polymers in various architectural forms, the flexible triboelectric nanogenerators (TENGs) have been extensively investigated. In this study, we design and fabricate lead-free $ZnSnO_3$ nanocubes @ polydimethylsiloxane (PDMS) based TENG by dispersing $ZnSnO_3$ nanocubes into PDMS elastomer at different ratios. Finally, the TENG can attain a maximum electrical output signal up to 400 V and 28 μA at a current density of 7 μA cm^{-2}, and an effective power to 3 mW at 6 wt% mass $ZnSnO_3$ mixed into PDMS. The harvested energy is utilized to drive 106 blue LEDs. In addition, this TENG generates stable electric power, even in the compressing-and-releasing process for over 500 cycles. Further investigation by electrostatic force microscopy shows clearly the maximum surface charge density appears at the optimal mixing ratio of $ZnSnO_3$ piezoelectric nanostructures into PDMS. This demonstrates that the optimization of the mixing ration between $ZnSnO_3$ piezoelectric nanostructures and PDMS is an effective method to increase the surface charges on the composite thin film and then improve the performance of the TENG. This TENG technology reveals a great candidate to be applied in large-scale device fabrications, flexible sensors and biological devices because of its easy fabrication process, high output power and biocompatibility.

Introduction

For the past few decades, significant attention has been attracted to harvest energy from the living environment as an alternative to solve the environmental problems as well as the energy crises [1-3]. Wang and co-workers showed the first nanogenerators (NGs) which converted energy directly from mechanical motion to electrical power in 2006 [4,5]. Since then, various structures of nanogenerators have been fabricated [6-8]. In particular, the flexible energy harvesters, which can be implanted in the human body (e.g. healing bone or tooth [9], monitoring the gentle motions of joints or even the Adam's apple

*Corresponding authors. Tel./fax: +86 23 65678362.
E-mail addresses: xiyi.xi@163.com (Y. Xi), phyliurc@cqu.edu.cn (R. Liu).

http://dx.doi.org/10.1016/j.nanoen.2015.09.012
2211-2855/

[10]) to convert to the electricity from more accessible mechanical energy sources without any restraints, have held great promise for realizing the energy generation from ambient environment. As we know, polydimethylsiloxane (PDMS) as a polymer electret would be desirable for the fabrication of the flexible devices due to its attractive properties such as flexibility, nontoxicity, cost-effectiveness, biocompatibility and transparency [11-14]. It can be also easily made into composite film by mixing nanoparticles or other nanostructures [15,16], which has been used extensively for nanogenerators [17,18], nanodevices [19] or nanosensors [20-22]. On the other hand, piezoelectric materials are one of the most interesting nanomaterials adopted in the energy-harvesting area because of their efficient ferroelectric constant [23-25]. However, in some of these piezoelectric nanomaterials (e.g. lead zirconate titanate (PZT)), lead can result in a high level of toxicity, so they are not ecologically friendly, while nonuniformity in the size and difficulty to control the morphology of nanostructures bring technical difficulty for other piezoelectric materials [26-28].

Recently, nanocomposite generators based on PDMS with a mixture of $ZnSnO_3$ have been reported [29,30]. S-W Kim et al. have reported on piezoelectric power generation based on high concentration $ZnSnO_3$ mixed into PDMS under high pressure [31]. Nevertheless, most of those studies have been focused on the piezoelectricity or piezoelectric nanogenerator, and limited result on the power generation has been obtained from a triboelectric nanogenerator (TENG) based on a composite consisting of a lower concentration of $ZnSnO_3$ in a lower frequency. In addition, the output performance of the TENG varies remarkably when changing the concentration of $ZnSnO_3$, but little is known about the dependency and it is still unclear how semiconductor $ZnSnO_3$ works in the polymer. Therefore, it is necessary to investigate the fundamental mechanism of the TENG based on a composite of a semiconductive material mixed into PDMS film.

Herein, based on triboelectrification of a dielectric composite film made of lead-free $ZnSnO_3$ nanocubes and PDMS, we report on a flexible, robust and cost-effective hybrid TENG. The output current, voltage and power of the TENG are quantitatively investigated by modifying PDMS with semiconductor $ZnSnO_3$ nanocubes in different mass ratios under different measuring frequencies, indicating the enhancement of the output power as compared with that of pure PDMS in the same design. Surprisingly, the higher power generation of the fabricated TENG can be realized in a lower frequency with a lower doped concentration. During the periodical compressing deformation, we have successfully obtained a stable maximum electrical signal that harvested up to 400 V and 28 μA at a current density of 7 μA cm^{-2}, and an effective power to 3 mW at a load resistance of ~20 MΩ, which has been used to illuminate at least 106 blue LEDs in series. The fundamental mechanism of the TENG is interpreted systematically by the surface charge density, as validated by the measurement of the surface charge density of the composite thin films by electrostatic force microscopy (EFM). In addition, the TENG shows good stability and durability. These results suggest that the fabricated flexible TENG is an excellent candidate to be applied in large-scale device fabrications, flexible sensors and biological devices, due to its easy fabrication and

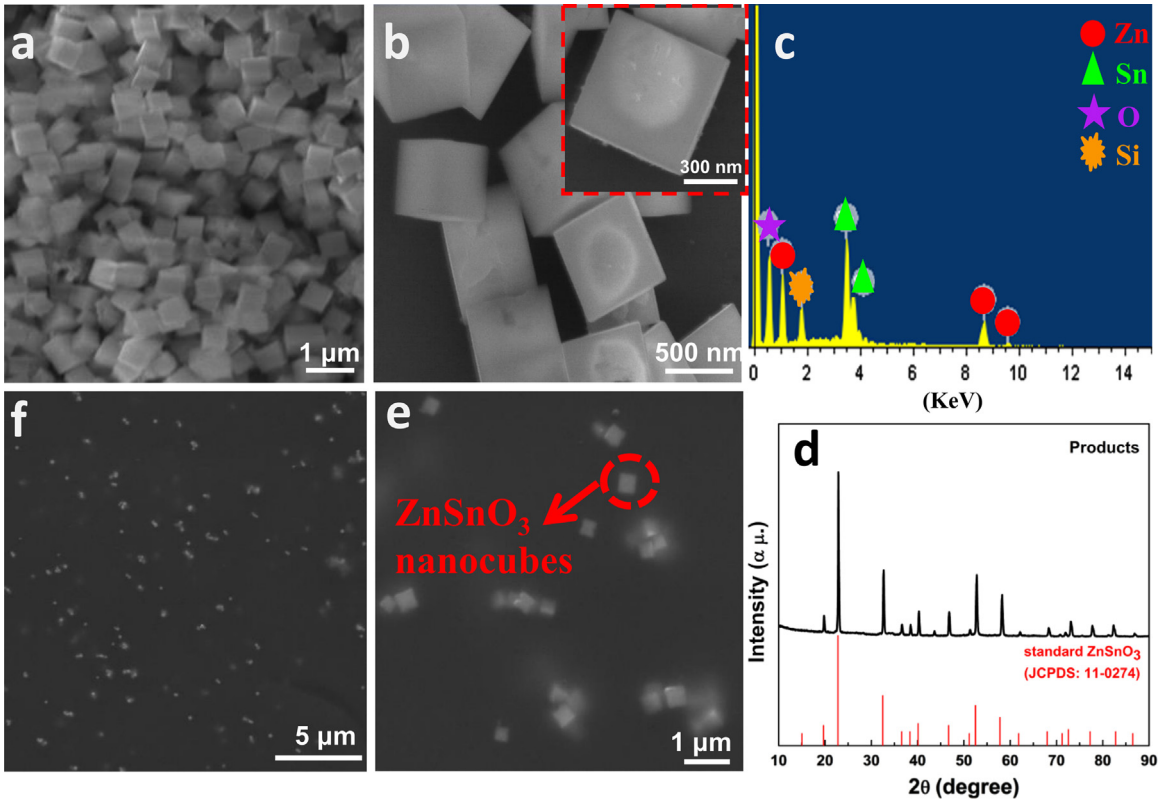

Figure 1 The SEM and FE-SEM images (a and b) and EDS spectra (c) of hydrothermally synthesized $ZnSnO_3$ nanocubes after cleaning how and drying steps. (d) XRD pattern of the $ZnSnO_3$ as-grown nanocubes. The cross-sectional (e) and surface (f) FE-SEM images of the the composite film.

process, high output power, remarkable durability and biocompatibility.

Experimental methods

Synthesis of $ZnSnO_3$ nanocubes

Single-crystalline $ZnSnO_3$ nanocubes were synthesized by hydrothermal method, which was displayed in S1.

Characterization of samples

The morphology and crystallinity of $ZnSnO_3$ nanostructures and composite film were analyzed by employing a scanning electron microscope (SEM, Nova 400) and a field-emission scanning electron microscope (FE-SEM, FEI Nova 400), respectively. The chemical compositions were analyzed by energy dispersive X-ray spectroscopy (EDS, Oxford). And the phase present of the $ZnSnO_3$ nanocubes were characterized by X-ray diffraction (XRD-6000, Shimadu, with Cu Kα radiation).

Fabrication of TENG

The TENG fabrication process can be summarized as the following. First, the PDMS (Sylgard 184, Dow Corning) was prepared by mixing base and curing agents at the weight percentage of 10/1 (w/w) and then the hydrothermally synthesized $ZnSnO_3$ nanocubes were dispersed into the PDMS elastomer at various concentrations of 2, 4, 6, 8, 10, 12, 20 and 25 wt%. Next, the mixture was prepared uniformly by pouring into a petri dish, stirring constantly and eliminating air bubbles. After curing in an oven at constant temperature of 55 °C for 2 h, the cured composite thin film with $ZnSnO_3$ clusters was peeled off from the petri dish and sliced into a size of 2×2 cm^2. This TENG device was fabricated by using a simple two-electrode system, where aluminum foils acted as electrodes separated by the working composite ($ZnSnO_3$@PDMS) thin film. The bottom electrode was pasted onto the PET substrate, the composite film was attached to it directly, and the upper electrode was independent with the surface of composite film by a gap. The electrical contact was taken from the bottom electrode and upper electrode with Cu wires, connected with double sided tape. Lastly, the whole device was placed in an oven again until it was completely cured molding. Then the TENG was fabricated.

Measurements of TENG and composite film

The output signals generated from the TENG device were measured by utilizing a linear motor (42HBS48BJ4-TR0), a Stanford low-noise current preamplifier (Model SR570), a Data Acquisition Card (NI PCI-6259) on a desktop PC and a Keithley 6514 system electrometer. The surface semi-

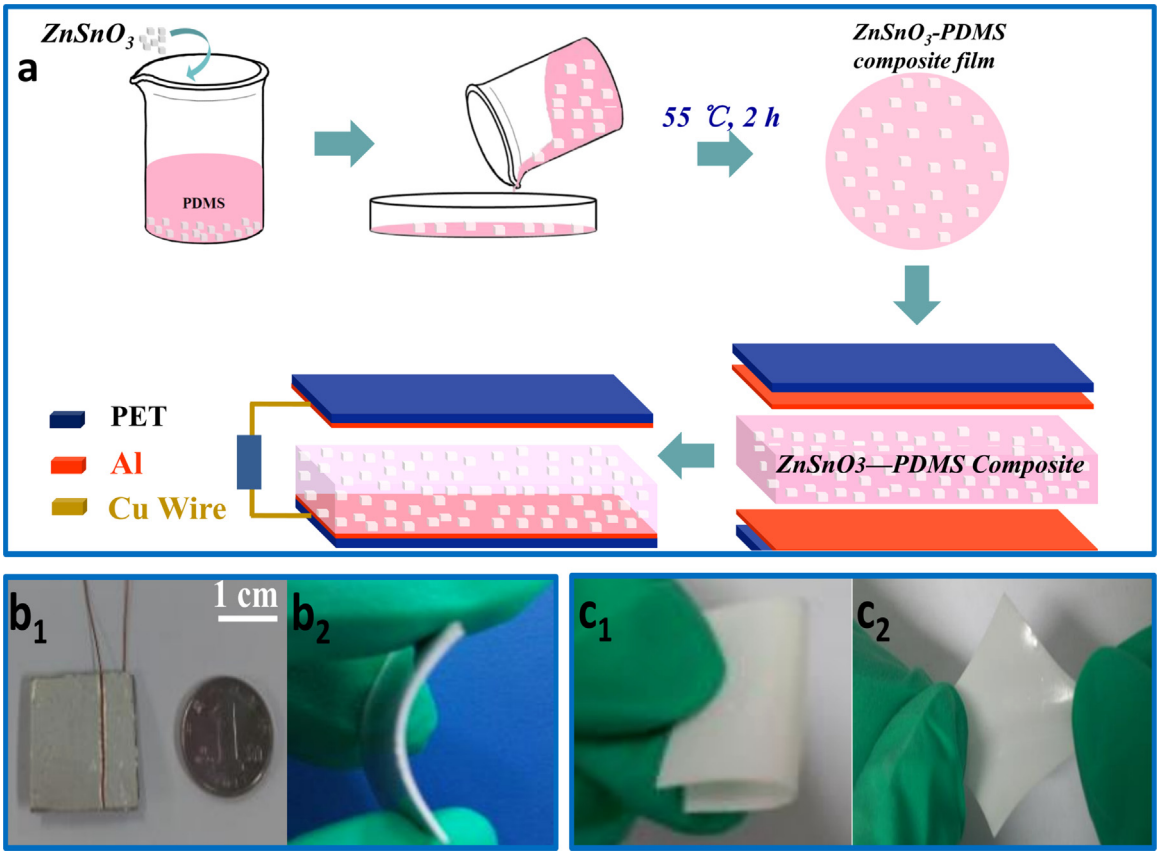

Figure 2 (a) Schematic diagram of the fabrication process of the TENG. (b_1) Photograph of a TENG device (2 cm × 2 cm). (b_2) A cross section of TENG completely bent by human fingers. Optical image of the $ZnSnO_3$-PDMS composite film at a rolled (c_1) and stretched (c_2) state, respectively.

quantitative charge information of the composite film was obtained by using Electrostatic force microscopy (EFM) that measurements were combined with atomic force microscopy (AFM, Asylum Research, MFP-3D) by utilizing conductive tips (Multi75 E-G, Budget Sensors).

Result and discussion

The microscopic surface morphology of the hydrothermally synthesized $ZnSnO_3$ is characterized by SEM and FE-SEM. The SEM image of the as-grown $ZnSnO_3$ obtained on a large scale after hydrothermal treatment at 160 °C for 14 h is shown in Figure. 1a. It can be observed that the products are composed of cubic-shaped $ZnSnO_3$ nanostructures. A typical high-magnification FE-SEM image shows the detailed morphologies of the prepared products, as shown in Figure. 1b, exhibiting a well-defined cubic nanostructure with similar side length of about 500–650 nm. An individual enlarged $ZnSnO_3$ cube image is provided in the inset of Figure. 1b, with a smooth surface and ruled edge apparently. The EDS results demonstrate that the contained elements are zinc, tin and oxygen in Figure. 1c (silicon is from the substrate). The XRD pattern is provided in Figure. 1d, which shows the perfect crystallinity and general results that all of the $ZnSnO_3$ diffraction peaks can be in accordance with standard $ZnSnO_3$ with the perovskite structures (JCPDS no. 11-0274). And no diffraction peaks from any other impurities are observed. The cross-sectional and surface FE-SEM images of the composite film are shown in Figure. 1e and f respectively, which display the $ZnSnO_3$ nanocubes can be well-distributed in a soft PDMS matrix. In addition, the $ZnSnO_3$ nanocubes are evenly distributed in the PDMS matrix, as evidenced by FE-SEM images and comparison tests of the TENG (Supplementary Figures. S1, S2, and S3).

As for energy harvesting, we adopt a widely used TENG fabrication technique. The schematic diagram of the fabrication process is detailed in Figure. 2a. Simply putting, this fabrication process could be divided into four steps. First, the synthesized $ZnSnO_3$ nanocubes are dispersed into PDMS elastomeric at various ratios to form a homogeneous mixture. Second, the composite film of $ZnSnO_3$ mixed with PDMS is formed and then cutted into an active device area of $2 \times 2\ cm^2$ after curing. Finally, the prepared composite thin film is assembled into the TENG with thick Al foil and PET substrate constituting a layer structure of two plates, which act as two opposite electrodes. Figure. $2b_1$ displays a photograph of a fabricated TENG device ($2 \times 2\ cm^2$), and the Figure. $2b_2$ shows an optical image of cross

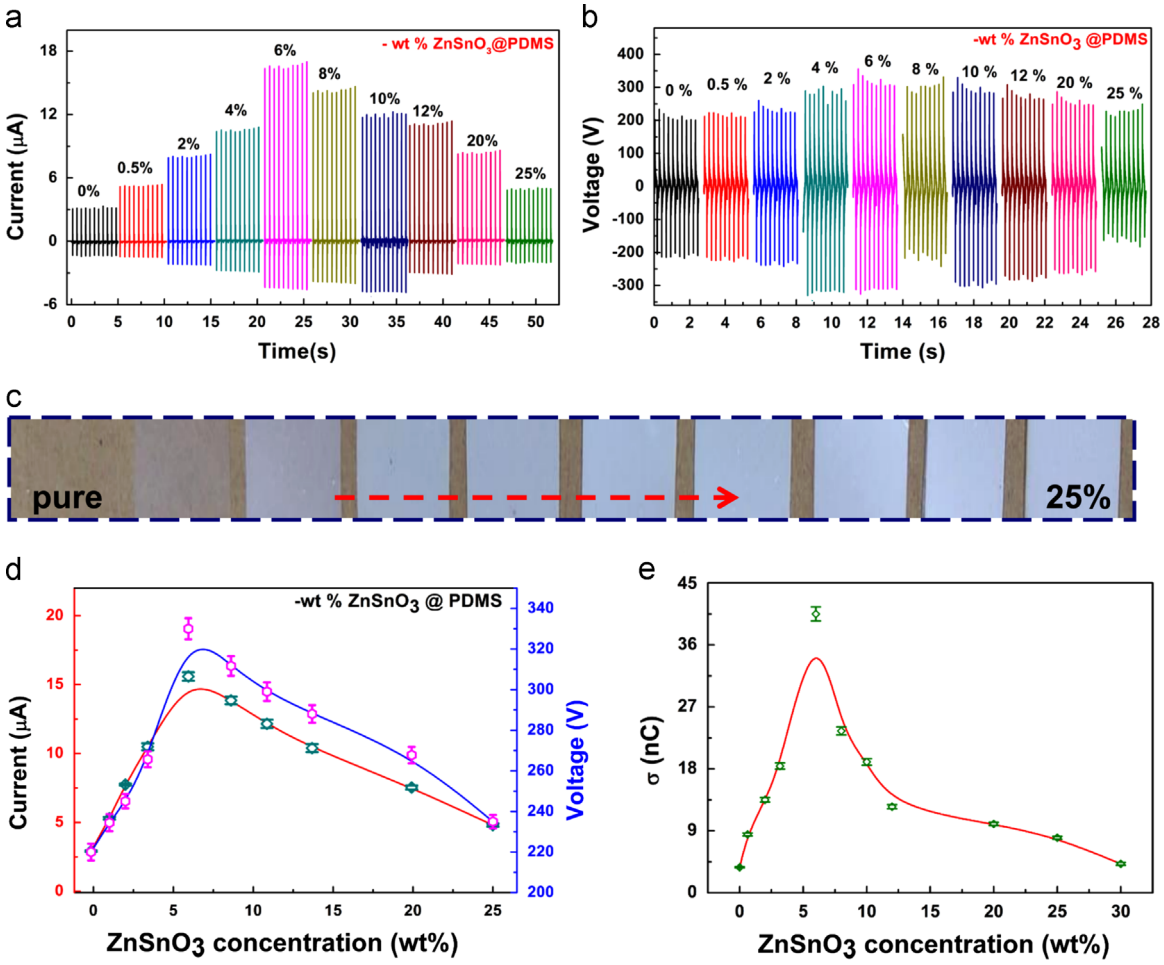

Figure 3 The harvested (a) output current and (b) voltage signals from TENG device with various ratios of $ZnSnO_3$ mixed with PDMS. (c) Digital image of the composite film with different doped $ZnSnO_3$ nanocubes concentrations. (d) Variation of current and voltage produced from TENG device with $ZnSnO_3$ concentration. (e) Variation of the composite film surface charge quantity with $ZnSnO_3$ concentration. The maximum obtained up to 40.5 nC with the $ZnSnO_3$ concentration of ~6%.

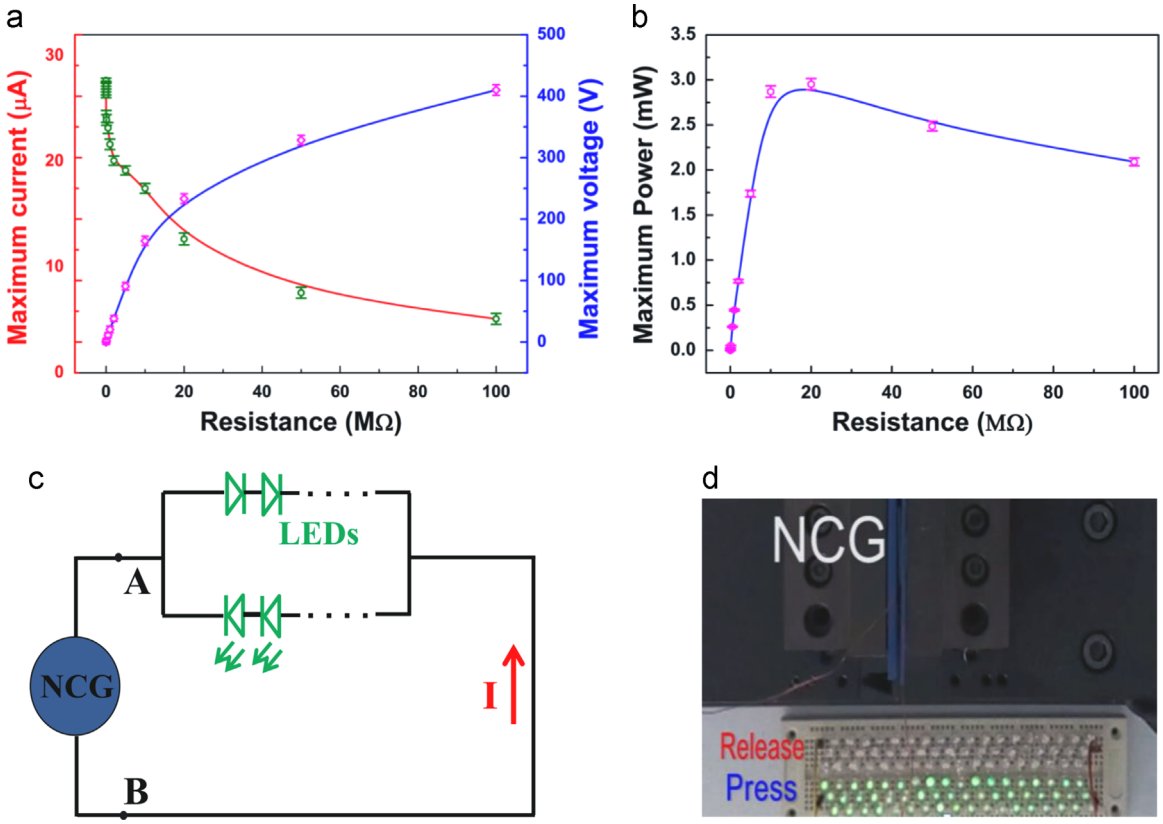

Figure 4 A maximum electrical signal generated from TENG: (a) The measured load voltage and current under the outer variable resistance from 10 Ω to 600 MΩ. (b) The relationship between the instantaneous power outputs and load resistance. The effective power harvested up to 3 mW at a load resistance of ~20 MΩ. A circuit diagram (c) and photograph (d) of blue LEDs being lit which are powered directly by the TENG.

section at a completely bent state by human fingers, exhibiting the flexibility of the device. Moreover, the photographs of the $ZnSnO_3$-PDMS composite film in Figure. 2c indicate that the composite film is remarkably flexible in different ways, such as rolling (Figure. $2c_1$) and stretching (Figure. $2c_2$), respectively.

To measure the electrical signals generated from the TENG, a linear motor, a current preamplifier, and a data acquisition card are used in this work. When the lead-free $ZnSnO_3$-PDMS TENG is regularly deformed by a liner motor in a fixed frequency of 2 Hz during the periodical mechanical compressing and releasing state, the uniform output current and voltage are attained in Figure. 3. To optimize the output performance, the fabricated TENG with various concentrations of $ZnSnO_3$ were fabricated with the same thickness and measured in the same conditions, as described in Fig. 3a and b. From these results, it can be seen that the generated output current and voltage are greatly enhanced in case of the working composite film with $ZnSnO_3$ nanocubes compared with the pure PDMS film. Moreover, the output signals increase with the $ZnSnO_3$ concentration until 6 wt%, and the generated output current of the harvester is gradually increased up to 16 μA, which is about more than five times of that of the pure PDMS film. Then further increment of $ZnSnO_3$ results in the gradual decrement of the output current to 5 μA at the doped concentration of 25 wt%, as described in Figure. 3a. The corresponding output voltage as shown in Figure. 3b exhibits a maximum up to 330 V. The photos of composite films with doped $ZnSnO_3$ concentration from 0 wt% to 25 wt% (Figure. 3c), indicate that the transparency of the films gradually decreases. In addition, Fig. 3d shows the dependency of the output current and voltage on the ratios of $ZnSnO_3$ nanocubes in the composite. Based on the output current in a half-cycle measurement (6% doped $ZnSnO_3$ concentration), the surface charge quantity of composite thin film is calculated as up to 40.5 nC, as shown in Fig. 3e.

Figure. 4a displays the output voltage and current as a function of load resistance from 10 Ω to 600 MΩ. When increasing the connected external resistance, the output current decreases but the output voltage increases. A maximum output up to 400 V and 28 μA can be generated from the TENG based on a composite film with 6 wt% of $ZnSnO_3$ and a thickness of 0.5 mm, which current is enhanced up to 6.2 times in comparison to that based on the pure PDMS (supplementary Figure. S4c). Finally, we characterize the instantaneous power outputs of the TENG by calculating the load voltage and current measured with the resistors (Figure. 4b), and the maximal electrical power is about 3 mW at a load resistance of ~20 MΩ and a test frequency of 2 Hz. This TENG can be used to illuminate 106 blue LEDs connected in series, as shown in Figure. 4d and video (in supporting information). And the Figure. 4c shows the corresponding circuit diagram.

Supplementary material related to this article can be found online at http://dx.doi.org/10.1016/j.nanoen.2015.09.012.

To prove the stability, the TENG is repeatedly compressed and released at a driving frequency of 1.5–3 Hz, for nearly 500 cycles (~250 s) per frequency. The steady output

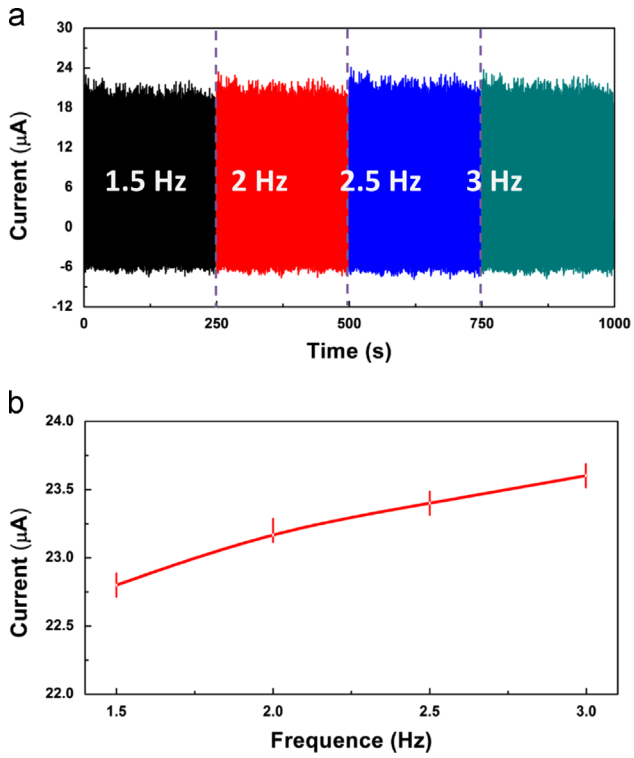

Figure 5 (a) The stability test of TENG in various driving frequencies. (b) The output current of TENG with an increase in driving frequency.

current (Figure. 5a) demonstrates the excellent stability of the TENG. The supplement for stability testing is also provided (Supplementary Figure. S5). In addition, slightly increment of the output current is found when the driving frequency increases from 1.5 Hz to 3 Hz (Figure. 5b).

The working mechanism of $ZnSnO_3$@PDMS (doped PDMS) TENG can be explained from the designed macro-structures and controlled micro dielectric materials of TENG, respectively. First, based on the design of the macro-structures, we can simply take the whole TENG as a flat-panel capacitor with an external load of R. Electron flow is driven back and forth through the external circuit in the pressing-and-releasing process of the TENG when it works, therefore, alternating current (voltage) pulse is formed. The schematic diagram of the doped PDMS TENG's cross-section is illustrated in Figure. 6a, where *L*, *D* represent the thickness of the composite thin film, the distance between the surface of the composite thin film and the bottom Al electrode, respectively. As shown in Figure. 6a, after a few times of pressing and releasing, the electron will be transferred from the Al electrode to the doped PDMS composite thin film, because the Al electrode loses electrons more easily than PDMS. However, as the PDMS is an organic dielectric electret material, the received electrons cannot be transferred or neutralized. Therefore, the electric charge distribution as shown in Figure. 6a(i) is formed. When $D \gg L$, due to the electrostatic induction, the top electrode has the same quantity of positive charge as the negative charge on the surface of the PDMS composite thin film. When *D* diminishes ($D \approx L$), the bottom electrode begins to induce charge. The electron flows from the bottom electrode to the top electrode, as shown in Fig. 6a(ii). And the positive charge on the top electrode will be completely neutralized by the electron coming from the bottom electrode until $D=0$, as shown in Figure. 6a(iii). If the pressing continues and the deformation of PDMS exceeds 0.52% [31], the electric dipoles inside $ZnSnO_3$ nanocubes will be oriented as shown in Figure. 6a(iv), due to the pressure induced polarization effect for the combination of organic and inorganic materials as well as the piezoelectric and ferroelectric nature of $ZnSnO_3$. Thus, a potential (ΔU) will be formed between the top and bottom electrodes, driving the electron flow from the bottom electrode to the top electrode and generating electricity flow. Besides, the time needed for pressing is extremely short, so the electrostatic induction occurs almost the same time as that of the pressure induced polarization effect, and the output current *I*, can be expressed as (Eq. (1))

$$I = \frac{dQ}{dt} = \frac{d(\sigma_1 + \sigma_2) \cdot S}{dt} = S\frac{d(\sigma_1 + \sigma_2)}{dt} \quad (1)$$

where *S* is the effective area, σ_1 is the induced charge and σ_2 is the polarization charge. Further, the releasing process is shown in Figure. 6a(v) and (vi), the releasing and pressing process are just in contrary situation and as the *dt* is greater than the pressing process, the current will be smaller than that coming out of the releasing process. Accordingly, with a periodic compressive force applied onto the TENG, a cyclic voltage and current output signals will be generated across the load between the electrodes.

Second, based on the controlled micro dielectric materials of TENG, we further discuss its mechanism. As we discussed, with an increase of doped $ZnSnO_3$ concentration in the PDMS matrix, the output performance of the TENG increased and reaches up to a maximum value of 330 V and 16μA. This is mainly due to the effects of bond breaking of Si-O-Si groups in the composite on the tribocharge generation property [32]. It is well known that PDMS is extremely sensitive to the free oxygen radicals, thus under the external driving force during the pressing process, on one hand, part of the PDMS methyl groups (Si-CH_3) breaks, on the other hand, reactive oxygen radicals produced by $ZnSnO_3$ nanocubes will attack some of the broken methyl groups (Si-CH_3) and substitute them with silanol groups (Si-OH), as shown in Figure. 6b. Accordingly, redundant dangling bonds will emerge in the way of electric charges, that is, the PDMS surface has been activated to be charged due to bond breaking and subsequent. Thus, with the increase of the amount of $ZnSnO_3$, the dangling bonds increase as well as the surface charge density increases gradually, further causing an increase of the output voltage/current. And the output maximizes when the concentration of $ZnSnO_3$ reaches up to 6%. However, when the doped amount of $ZnSnO_3$ continues to increase, the output begins to decrease. This is because the tribocharge generation of the PDMS surface due to the bond breaking of Si-O-Si groups has already reached a saturated point. In this case, further increment of $ZnSnO_3$ in the PDMS matrix attenuates the output signal as the relative permittivity of $ZnSnO_3$ becomes the main factor and affects the surface charge density. Herein, based on Gauss theorem and Ampere cycle theorem in the static electricity field, we can explain the surface charge density σ_{Al} on the Al foil electrode as follows [33]

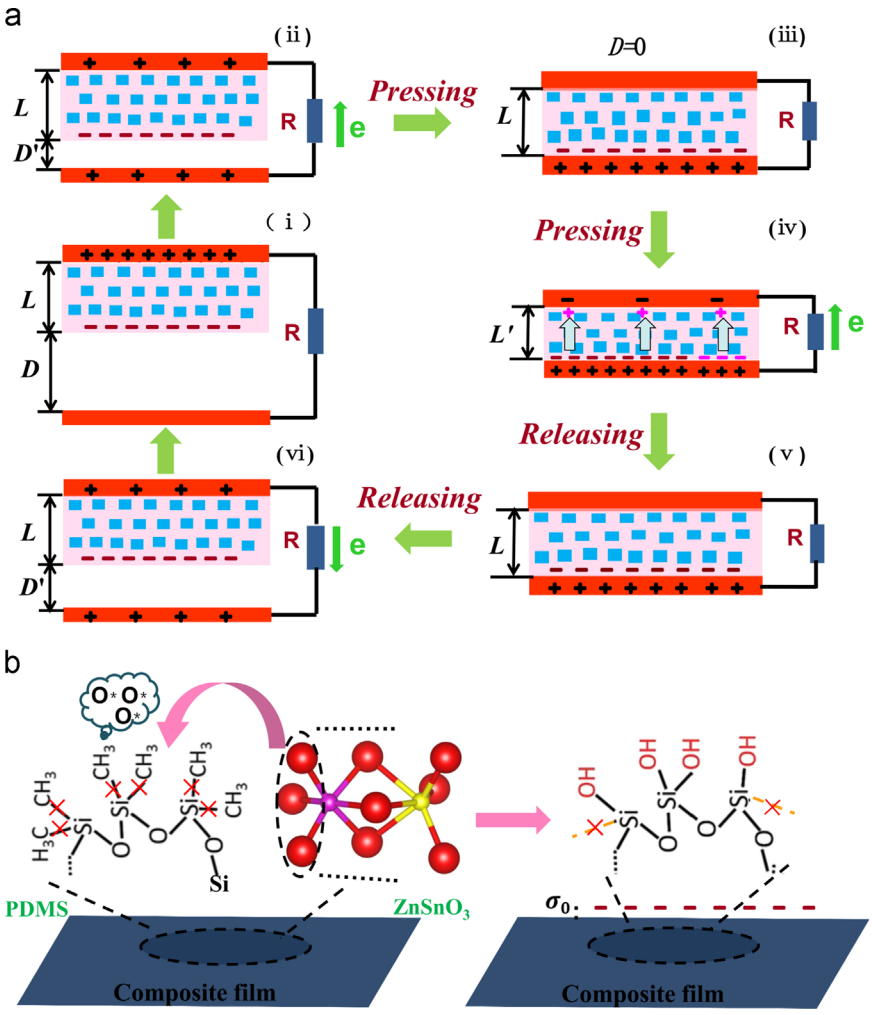

Figure 6 Working mechanism of this TENG device: (a) The cross-sectional schematic diagram of the TENG under a cyclic compressive force in the macro-structure. The schematic diagram of charge distribution and current direction when the TENG device is (i) at initial state with no force applied, (ii) being pressed gradually, (iii and iv) pressed completely, and (v and vi) released. (b) Schematic illustration of the charges in the molecular structure of the PDMS and $ZnSnO_3$ based on the controlled micro dielectric material.

(Eq. (2))

$$\sigma_{Al} = \frac{\sigma_0}{1 + \frac{(\varepsilon_{ZnSO3} + \varepsilon) \cdot D}{L}} \tag{2}$$

where σ_0 is the surface charge density of the composite film, L is the thickness of composite film, ε_{ZnSnO3} is the relative permittivity of $ZnSnO_3$, ε is the relative permittivity of PDMS and D denotes the distance between the composite PDMS surface and Al foil layer. As mentioned above, in the same situation, when the amount of doped $ZnSnO_3$ increases, the relative permittivity of $ZnSnO_3$ ε_{ZnSnO3} plays the major role, causing the decrease of σ_{Al} and resulting in a decrease of the output signals. The same conclusion has also been verified in the measuring the surface charge density of the composite film by electrostatic force microscopy (EFM).

To validate the surface charge dependency on the $ZnSnO_3$ ratios in the composite thin films, further measurements by EFM were carried out. The interleaved EFM measurements were performed according to the way as described by Yalcin *et al.* [34]. The results are shown in Figure 7a, where the blue, green, red and black line correspond to the phase shift of 2%, 4%, 6% and 8% $ZnSnO_3$-PDMS composite film, respectively. The measured EFM data is fitted by the following polynomial equation (Eq. (3)),

$$\Delta\Phi = K_0 + K_1 V_{EFM} + K_2 V_{EFM}^2 \tag{3}$$

where $\Delta\Phi$ is the phase shift of the resonant peak (degree) [35], while K_0, K_1 and K_2 are defined as $K_1 = [Q/(kz^2)]q$ and $K_2 = -(Q/k)[(3\alpha)/z^4]$ [36], where Q is the quality factor, k is the spring constant of the cantilever, z is the tip-surface distance, q is the surface charge, α is the electric polarizability. (In this study, $Q=175$, $k=2.8$ N/m and $z=50$ nm, and the relative errors are less than 1%). Thus, from the fitting to Figure. 7a, the surface charges in these samples can be evaluated, as shown in Figure. 7b. Because the same cantilever and tip are used across all the samples, the surface charges obtained are also proportional to the surface charge density of the sample (supplementary S5). In Figure. 7b, it is clear that the surface charge reaches up to the maximum at a doped $ZnSnO_3$ concentration of 6%. This is the same as the dependency of the output current/voltage on the $ZnSnO_3$ nanocubes ratio in the composite thin film, as

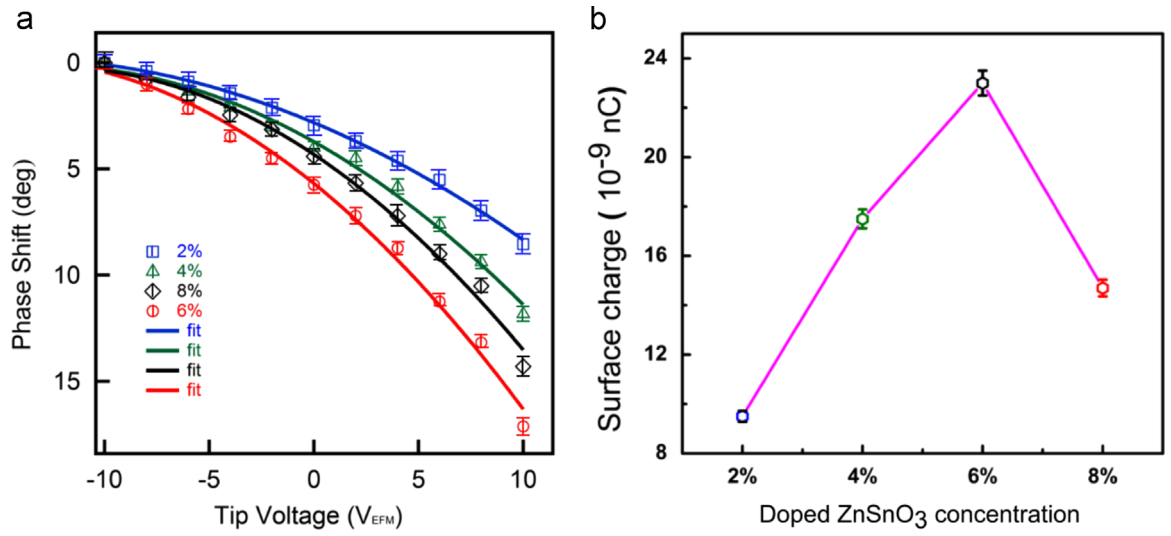

Figure 7 The dependency of the surface charge measured by EFM on the composite concentration in the thin films. (a) Phase shift vs VEFM measured for composite film with different concentration of $ZnSnO_3$ nanocubes. (b) Surface charge calculated from EFM measurement for the composite thin film depends on the doped $ZnSnO_3$ nanocubes concentration.

shown in Fig. 3d and e. All these results are in conformity with the experimental conclusion, thus verifying the mechanism proposed. Hence, the output current varies with the different doped ratios and 6% is the optimal doped ratio of $ZnSnO_3$ nanocubes, as proved in Fig. 3a and b. Herein, we obtain a clear understanding about the performance of the TENG that optimization of the mixing ration between lead-free $ZnSnO_3$ piezoelectric materials and PDMS is an effective method to modify PDMS and an important factor to improve the performance of the composite PDMS-based TENG.

Conclusion

In summary, we have reported a high-performance and lead-free TENG incorporating the piezoelectric $ZnSnO_3$ nanocubes and PDMS. The flexible, robust and cost-effective TENG can harvest stable electrical outputs during the periodical mechanical compressing and releasing state. To develop the performance of the fabricated TENG, we optimized the mixing ratio between lead-free $ZnSnO_3$ nanocubes and organic polymers, and the thickness of composite thin film. Finally it is demonstrated that the composite film with a doped $ZnSnO_3$ concentration of 6 wt% and a thickness of 0.5 mm can produce a maximum electrical output signal up to 400 V, 28 μA at a current density of 7 μA cm^{-2}, and an effective power up to 3 mW at a load resistance of ~20 MΩ, which has been used to illuminate at least 106 blue LEDs in series. Compared with the pure PDMS film-based nanogenerator, the TENG's performance is greatly enhanced with a greater output current, which is up to 6.2 times. This working mechanism has also been verified by using an EFM to measure the surface charge of the composite film, correspondingly. The flexible TENG technology reveals remarkable advantages as easy fabrication, high-performance and biocompatibility, which is an excellent candidate for large-scale device fabrications, flexible sensors and biological devices,

Acknowledgments

This work has been funded by the NSFC (11204388), the SRFDP (20120191120039), the NSFCQ (cstc2014jcyjA50030), the Development Program ("863" Program) of China (2015AA034801), the Fundamental Research Funds for the Central Universities (No. CQDXWL-2014-001, CQDXWL-2013-012, 106112015CDJXY300004), the large-scale equipment sharing fund of Chongqing University, and the Chongqing University Postgraduates' Innovation Project (No. CYS15016).

Appendix A. Supplementary material

Supplementary data associated with this article can be found in the online version at http://dx.doi.org/10.1016/j.nanoen.2015.09.012.

References

[1] A.Z. Abidin, T. Puspasari, W.A. Nugroho, Proc. Chem. 4 (2012) 11–16.
[2] S.W. Chen, C.Z. Gao, W. Tang, H.R. Zhu, Y. Han, Q.W. Jiang, T. Li, X. Cao, Z.L. Wang, Nano Energy 14 (2015) 217–225.
[3] X.Y. Xue, W.L. Zang, P. Deng, Q. Wang, L.L. Xing, Y. Zhang, Z. L. Wang, Nano Energy 13 (2015) 414–422.
[4] Z.L. Wang, J.H. Song, Science 312 (2006) 242–246.
[5] S. Xu, B.J. Hansen, Z.L. Wang, Nat. Commun. 1 (2010) 93.
[6] Z.H. Li, G. Cheng, X.H. Li, P.K. Yang, X.N. Wen, Z.L. Wang, Nano Energy 15 (2015) 256–265.
[7] J.M. Wu, C. Xu, Y. Zhang, Y. Yang, Y. Zhou, Z.L. Wang, Adv. Mater. 24 (2012) 6094–6099.
[8] T.C. Hou, Y. Yang, H. Zhang, J. Chen, L.J. Chen, Z.L. Wang, Nano Energy 2 (2013) 856–862.
[9] W. Tang, J.J. Tian, Q. Zheng, L. Yan, J.X. Wang, Z. Li, Z. L. Wang, ACS Nano 9 (2015) 7867–7873.
[10] P.K. Yang, L. Lin, F. Yi, X.H. Li, K.C. Pradel, Y.L. Zi, C. Wu, J. H. He, Y. Zhang, Z.L. Wang, Adv. Mater. (27) (2015) 3817–3824.
[11] J.S. Chun, N.R. Kang, J.Y. Kim, M.S. Noh, C.Y. Kang, D. Choi, S. W. Kim, Z.L. Wang, J.M. Baik, Nano Energy 11 (2015) 1–10.

[12] C.K. Jeong, K. Park, J. Ryu, G.T. Hwang, K.J. Lee, Adv. Funct. Mater. (24) (2014) 2620–2629.
[13] Y.H. Ko, G. Nagaraju, S.H. Lee, J.S. Yu, Appl. Mater. Interfaces (6) (2014) 6631–6637.
[14] J.W. Zhong, Y. Zhang, Q. Zhong, Q.Y. Hu, B. Hu, Z.L. Wang, J. Zhou, ACS Nano (8) (2014) 6273–6280.
[15] H. Sun, H. Tian, Y. Yang, D. Xie, Y.C. Zhang, X. Liu, S. Ma, H. M. Zhao, T.L. Ren, Nanoscale (5) (2013) 6117–6123.
[16] K.I. Park, M. Lee, Y. Liu, S. Moon, G.T. Hwang, G. Zhu, J. E. Kim, S.O. Kim, D.K. Kim, Z.L. Wang, K.J. Lee, Adv. Mater. (24) (2012) 2999–3004.
[17] Z.H. Lin, G. Cheng, Y. Yang, Y.S. Zhou, S. Lee, Z.L. Wang, Adv. Funct. Mater. (24) (2014) 2810–2816.
[18] Z.H. Lin, Y. Yang, J.M. Wu, Y. Liu, F. Zhang, Z.L. Wang, J. Phys. Chem. Lett. (3) (2012) 3599–3604.
[19] B. Bhushan, D. Hansford, K.K. Lee, J. Vac. Sci. Technol. A (24) (2006) 1197–1202.
[20] B. Saravanakumar, S. Soyoon, S.J. Kim, ACS Appl. Mater. Interfaces (6) (2014) 13716–13723.
[21] B. Zhang, Z.M. Xiang, S.W. Zhu, Q.Y. Hu, Y.Z. Cao, J.W. Zhong, Q.Z. Zhong, B. Wang, Y.S. Fang, B. Hu, J. Zhou, Z.L. Wang, Nano Res. (7) (2014) 1488–1496.
[22] Y. Yang, H.L. Zhang, J. Chen, S.M. Lee, T.C. Hou, Z.L. Wang, Energy Environ. Sci. (6) (2013) 1744–1749.
[23] S. Xu, Y. Yeh, G. Poirier, M.C. McAlpine, R.A. Register, N. Yao, Nano Lett. 13 (2013) 2393–2398.
[24] X.M. He, H.Y. Guo, X.L. Yue, J. Cao, Y. Xi, C.G. Hu, Nanoscale (7) (2015) 1896–1903.
[25] S.H. Shin, Y.H. Kim, M.H. Lee, J.Y. Jung, J. Nah, ACS Nano (8) (2014) 2766–2773.
[26] P.K. Panda, J. Mater. Sci. (44) (2009) 5049–5062.
[27] P.K. Panda, B. Sahoo, Ferroelectrics (474) (2015) 128–143.
[28] Ü. Özgür, Y.I. Alivov, C. Liu, A. Teke, M.A. Reshchikov, S. Doğan, V. Avrutin, S.J. Cho, H. Morkoç, J. Appl. Phys. (98) (2005) 041301–041403.
[29] J.M. Wu, C. Xu, Y. Zhang, Z.L. Wang, ACS Nano (6) (2012) 4335–4340.
[30] M.M. Alam, S.K. Ghosh, A. Sultana, D. Mandal, Nanotechnology 26 (2015) 165403–165408.
[31] K.Y. Lee, D. Kim, J.H. Lee, T.Y. Kim, M.K. Gupta, S.W. Kim, Adv. Funct. Mater. (24) (2014) 37–43.
[32] F.R. Fan, J.J. Luo, W. Tang, C.Y. Li, C.P. Zhang, Z.Q. Tian, Z. L. Wang, J. Mater. Chem. A (2) (2014) 13219–13225.
[33] Y. Suzuki, IEEJ Trans. Electr. Electron. Eng. (6) (2011) 101–111.
[34] S.E. Yalcin, J.A. Labastide, D.L. Sowle, M.D. Barnes, Nano Lett. (11) (2011) 4425–4430.
[35] T. Heim, K. Lmimouni, D. Vuillaume, Nano Lett. (4) (2004) 2145–2150.
[36] J. Kim, W.J. Jasper, J.P. Hinestroza, J. Eng. Fibers Fabr. (1) (2006) 30–46.

Guo Wang is currently pursuing her Master degree under the supervision of Prof. Yi Xi in Condensed Matter Physics, Chongqing University. Her research interests are mainly focused on nanogenerator.

Yi Xi received her Ph.D. in 2010 in Physics from Chongqing University, China. Now she is an associate professor at Chongqing University, China. Her main research interests focus on the fields of piezoelectric, triboelectric nanogenerators for energy harvesting and supercapacitors for energy storage, driving some personal electronic devices.

Haixia Xuan is currently pursuing her Master degree under the supervision of Prof. Ruchuan Liu at the Physics Department of Chongqing University. Her research interests mainly focus on the application of AFM based technology.

Ruchuan Liu received his Ph.D. in 2004 in Physical Chemistry from Columbia University at New York, USA. Now he is a principal investigator at Chongqing University, China. His research interests focus on photovoltaic materials, biomaterials, nano/molecular devices, especially the underline molecular mechanism.

Xi Chen received his B.S. degree from the Department of Applied Physics at the Chongqing University in 2013. He is currently pursuing his Master degree under the supervision of Prof. Ruchuan Liu at the Physics Department of Chongqing University. His research interests mainly focus on the application of AFM based technology.

Cheng Lu, who received B.S. degree in Applied Physics (2013) from Chong Qing University. Now, she is a postgraduate student in Chong Qing University. Her research interests are mainly focused on nanogenerator.